IEEE Access
Multidisciplinary | Rapid Review | Open Access Journal

Received December 27, 2020, accepted January 14, 2021, date of publication January 19, 2021, date of current version February 3, 2021.

Digital Object Identifier 10.1109/ACCESS.2021.3052944

Sliding-Mode Clamping Force Control of Electromechanical Brake System Based on Enhanced Reaching Law

YIYUN ZHAO, HUI LIN, AND BINGQIANG LI
School of Automation, Northwestern Polytechnical University, Xi'an 710129, China
Corresponding author: Yiyun Zhao (zhaoyiyun@mail.nwpu.edu.cn)

This work was supported in part by the National Natural Science Foundation of China under Grant 51777170, and in part by the Natural Science Basic Research Plan in Shaanxi Province of China under Grant 2019JM-462 and Grant 2020JM-151.

ABSTRACT The control of clamping force has a significant influence on the braking performance of low-floor trams. However, the load torque variations, strong nonlinearity and complex structure of electromechanical brake (EMB) systems present challenging the clamping force control issues. In this paper, an EMB system mathematical model is established. Then, an enhanced sliding-mode reaching law (ESMRL) is investigated to address these issues. In addition, novel gap distance elimination and adjustment strategies are proposed to improve the response quality and adjust the gap distance in a simple and low-cost way. Taking advantages of minimal chattering and short reaching times, the proposed ESMRL enhances the dynamic performance and tracking accuracy of the clamping force control. Finally, simulation and experimental results are offered to validate the effectiveness and superiority of the proposed control strategy.

INDEX TERMS Electromechanical brake (EMB), sliding-mode control (SMC), sliding-mode reaching law (SMRL), clamping force control, gap distance control.

I. INTRODUCTION

As an eco-friendly mode of transportation, low-floor trams are vital components of urban rail transit systems [1]. Because their operating routes interact with pedestrians and vehicles, low-floor trams operating environments are complicated. Hence, the safety and reliability of their brake systems are of utmost importance [2], [3].

Conventional braking systems for low-floor trams can divided into two types: air braking systems and hydraulic braking systems [4]. With the development of mechatronic servo system designs and high-performance control technologies, EMB systems have been gaining popularity in train braking systems [5], [6]. Compared with a conventional braking system, an EMB system has several advantages: 1) faster response; 2) higher maintainability; 3) lighter weight; 4) improved economy [7], [8].

EMB control relies on a mechatronic servo control of the clamping force. The actual systems feature nonlinear characteristics such as load torque variations, strong nonlinearity and complex structures [9], [10]. Therefore, the strong nonlinearity is an important factor challenging the control in industrial applications, and a conventional control strategy cannot obtain an ideal high-precision control performance [11]–[13]. Over recent years, various control strategies have been presented to improve the performance of mechatronic servo systems, such as adaptive backstepping control [14], adaptive linear active disturbance rejection control [15], adaptive terminal sliding-mode control [16] and model predictive control [17].

As a nonlinear control method, sliding-mode control (SMC) has the merits of fast global convergence, strong robustness and simplicity of realization [18]–[22]. Therefore, SMC has been successfully applied in various fields, such as robot control [23], [24], satellite attitude control [25], electromagnet levitation control [26] and mechatronic servo control [16]. However, due to the existence of switching time delays, measuring errors and additional factors in practical application, the chattering phenomenon is an inherent attribute of SMC [27]–[29]. This can influence the accuracy of control and cause a system to oscillate. In previous studies, various control strategies have been proposed to mitigate

The associate editor coordinating the review of this manuscript and approving it for publication was Zhe Xiao.

the chattering phenomenon and accelerate the convergence rate. In [30], Feng *et al.* proposed a full-order sliding-mode control strategy. Junejo *et al.* proposed an adaptive terminal sliding-mode reaching law [31]. A nonsingular terminal sliding-mode control strategy was suggested by Yi *et al.* in [32]. YE *et al.* proposed a robust adaptive sliding-mode control strategy [33].

When implementing these control strategies, the reaching law approach can directly obtain command of the approaching process to mitigate the chattering phenomena and accelerate the convergence rate. In [34], Gao *et al.* proposed a constant-proportional rate reaching law for robot manipulators. However, the coefficients of the reaching law were constant, and the reduced chattering was not distinct. Based on the conventional exponential reaching law, Wang *et al.* introduced a system state variable and a power order term of a sliding-mode function to propose a new reaching law. The superiority of this reaching law approach was verified in the permanent magnet synchronous motor (PMSM) speed regulation system [35]. Brahmi *et al.* employed a damping sinusoid to propose an adaptive reaching law to mitigate the chattering phenomenon and shorten the reaching time of the state variable to the sliding-mode surface. The reaching law was applied in an electric cylinder, and experimental results confirmed the feasibility and simplicity of this approach [36]. Tao *et al.* proposed a double hyperbolic reaching law to achieve a fast converging and chatter-free sliding-mode control. The lack of experimental verification was a major drawback of this strategy [37]. However, most of the proposed reaching laws have been verified by theoretical analysis and simulation. There is a lack of relevant experimental studies. Moreover, there are few studies applying the reaching law approach in EMB systems.

To prevent friction between the brake disc and pad when the low-floor tram is running, an adequate gap distance must be maintained. With increased use, worn brake disks and pads will lead to an increased gap distance. This can lead to a slow braking response in the system, and the different response time may lead to side slippage, derailing or other hazardous conditions. In [38], Shin *et al.* crafted a mechanism to carry out an adjustment strategy, which led to increased installation space. With limited installation space, this is difficult to implement in a low-floor tram. Few studies have focused on the elimination of gap distance.

Motivated by the above work, and in order to further improve the dynamic performance of the EMB system, an ESMRL is proposed. The proposed ESMRL can not only suppress the chattering phenomenon but also accelerate the state variable to reach the sliding-mode surface. Meanwhile, to ensure the reliable operation of a low-floor tram EMB system, this paper proposes strategies related to gap distance control. The main contributions of the proposed article are as follows:

1) A mathematical model of an EMB system is established.

2) An ESMRL is proposed to mitigate the chattering phenomena and accelerate the convergence rate of the state variable to the sliding-mode surface. In addition, the superiority of the ESMRL is verified by theoretical analysis.

3) A sliding-mode clamping force controller based on the ESMRL is designed for the EMB system.

4) Novel elimination and adjustment strategies of gap distance are proposed to improve the response quality

5) To adjust the gap distance without an extra mechanism, a gap distance adjustment control strategy is proposed.

6) The proposed control strategies are verified in simulations and experiments.

The remainder of this article is organized as follows: Section II illustrates the mathematical model of the EMB system. The performance analysis of the proposed ESMRL is elaborated in Section III. Section IV outlines the gap distance elimination and adjustment strategy. Then, the simulation and experimental results are presented to verify the superiority and effectiveness of the ESMRL in Section V. Section VI finally summarizes the paper and addresses the directions to further work.

II. MATHEMATICAL MODEL OF EMB SYSTEM

The EMB system of the low-floor tram investigated in this paper is shown in Fig. 1. The EMB system is composed of an electromechanical actuator (EMA), a brake disc, a brake clamp structure, and an EMA controller.

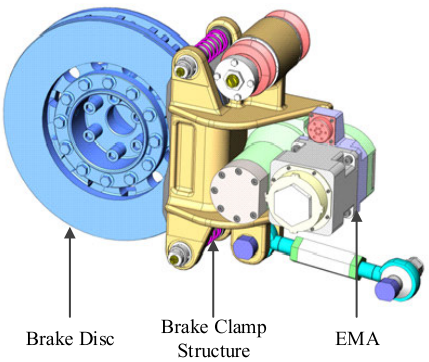

FIGURE 1. EMB system of low-floor tram.

As the major driving element of the EMA, the brushless DC motor (BLDCM) drives the screw nut through the planetary gear, which transforms the rotational motion into linear motion. Then, the ball screw pushes the lever, which makes the brake pad produce friction torque with the brake disc under the action of thrust. The common, emergency and parking braking modes of urban rail trains will be realized. The structure of the EMA is shown in Fig. 2.

To facilitate the analysis, the following assumptions are made:

Assumption 1: The saturation of the motor stator core is ignored, and the cogging effect and armature reaction are omitted.

Assumption 2: There is no eddy current or magnetic hysteresis loss.

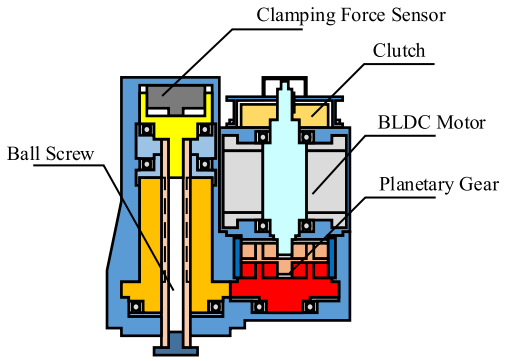

FIGURE 2. Structure of the EMA.

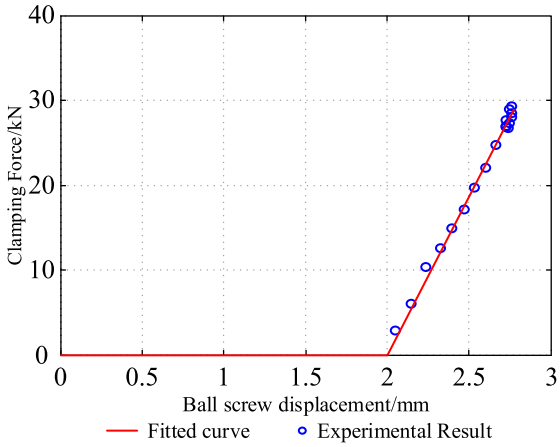

FIGURE 3. Stiffness curve of the EMB system.

Assumption 3: The armature winding is regarded as evenly distributed in the stator inner surface.

The mathematical model of the BLDCM can be expressed as follows:

$$\begin{cases} U_d = R_m i + L\dot{i} + K_e \omega_m \\ J\dot{\omega}_m = K_T i - T_L - B_v \omega_m \end{cases} \tag{1}$$

where, U_d represents the armature voltage. R_m represents the stator resistance. i represents the armature current. J represents the rotary inertia. ω_m represents the actual motor speed. T_L represents the load torque. B_v represents the viscous friction coefficient. K_T represents the torque constant. K_e represents the EMF constant.

The ball screw converts the rotational motion of the planetary gear into axial motion. Regardless of the elastic deformation, the kinematic equation is designed as follows:

$$x_{EMA} = \frac{\theta_m L_0}{2\pi GR} \tag{2}$$

where, x_{EMA} represents the displacement of the ball screw. θ_m represents the rotation angle of the motor shaft. L_0 represents the lead of the ball screw. GR represents the reduction ratio of the planetary gear.

Considering the brake pad deformation and the clearance of the system, the stiffness curve of the EMB system is shown in Fig. 3.

To avoid friction between the brake pad and disc, a sufficient gap distance should be maintained between them. The gap distance is a significant factor in the mathematical model of the EMB system.

By fitting the experimental result, the approximate mathematical relationship, which considers the gap between the brake pad and disc, between the displacement of the ball screw and the clamping force is as follows:

$$\begin{cases} F_{EMA} = k_s \left(x_{EMA} - D\right), & \left(x_{EMA} \geq D\right) \\ F_{EMA} = 0, & \left(0 \leq x_{EMA} < D\right) \end{cases} \tag{3}$$

where, D represents the gap distance between the brake gap and disc.

The clamping force on the brake disc is driven by the ball screw, and the load of the drive motor can be represented as

$$F_{EMA} = \frac{2\pi GR}{L_0} T_l \tag{4}$$

III. PROPOSED ENHANCED SLIDING-MODE REACHING LAW

A. CONVENTIONAL SLIDING-MODE REACHING LAW

A routine design method of a sliding-mode controller involves two steps: designing the sliding-mode surface and designing the reaching law. An appropriate reaching law design can reduce the chattering phenomenon and accelerate the convergence rate of the system.

For the most part, a conventional sliding-mode reaching law (CSMRL) can be used in engineering applications, which can be expressed as

$$\dot{s} = -\varepsilon_0 \mathrm{sgn}\left(s\right) \tag{5}$$

where $\varepsilon_0 > 0$.

For the CSMRL, ε_0 represents the reaching rate of the state variable. This means that the state variable will reach the sliding face at a constant speed.

The reaching time of the CSMRL is derived as

$$t_{rtc} = \frac{\left|s\left(0\right)\right|}{\varepsilon_0} \tag{6}$$

The discrete form of the CSMRL is expressed as

$$s\left(n+1\right) - s\left(n\right) = -\varepsilon_0 T_0 \mathrm{sgn}\left(s\left(n\right)\right) \tag{7}$$

where T_0 is the sampling period.

$$\begin{cases} s\left(n+1\right) = -\varepsilon_0 T_0, & s\left(n\right) = 0^+ \\ s\left(n+1\right) = \varepsilon_0 T_0, & s\left(n\right) = 0^- \end{cases} \tag{8}$$

Based on (8), the sliding boundary width of the CSMRL is derived as

$$\Delta_{CSMRL} = 2\varepsilon_0 T_0 \tag{9}$$

It can be seen from equation (6) that the reaching time of the CSMRL is related to the reaching rate ε_0. Nevertheless, there is a contradiction between the system chattering and reaching time. If the parameter ε_0 increases, the reaching time of the state variable to the sliding-mode surface will be shorter, and the chattering phenomenon will be aggravated.

B. PROPOSED ENHANCED SLIDING-MODE REACHING LAW

To achieve better speed control performance, a novel sliding-mode reaching law (NSMRL) is proposed in [39]. It is given by

$$\dot{s} = -\frac{\varepsilon_N}{\delta_N + \gamma_N e^{-\alpha_N |s|}} \operatorname{sgn}(s) \tag{10}$$

where, $\varepsilon_N > 0, 0 < \delta_N < 1, \gamma_N > 0$ and $\alpha_N > 0$.

However, the disadvantage of the NSMRL is that the reaching law cannot be adjusted.

Motived by the NSMRL, the ESMRL is proposed to improve the dynamic and weaken the inherent chattering, which can be expressed as

$$\begin{cases} \dot{s} = -\Psi(x, s) \operatorname{sgn}(s) - \eta |x|^m s \\ \Psi(x, s) = \dfrac{\varepsilon}{\delta + \left(1 + \frac{1}{|x|^n} - \delta\right) e^{-\alpha |s|}} \\ \lim\limits_{t \to \infty} |x| = 0 \end{cases} \tag{11}$$

where, s represents the sliding-mode surface. x represents the system state variable. $\varepsilon > 0, 0 < \delta < 1, n \geq 1, \alpha > 1, \eta > 0$ and $0 < m < 2$.

When the state variable is far away from the sliding-mode surface, $|s|$ is sufficiently large, and the term $e^{-\alpha|s|}$ will be extraordinarily small. Therefore, the denominator of $\Psi(x, s)$ converges to δ, and $\Psi(x, s)$ is equal to ε/δ. It has a faster reaching rate to make the state variable approach the sliding-mode surface. When the state variable approaches the sliding-mode surface, the value of s and x are approximately equal to 0, and thus $\Psi(x, s)$ is equal to 0. The reaching speed will decrease gradually. This means that when the variable reaches the sliding-mode surface, $\Psi(x, s)$ converges to 0, and the chattering phenomenon will be weakened. Considering the second term of ESMRL, $|x|^n$ ensures a large reaching rate at the initial state. As the state variable converges to 0, the reaching rate also decreases to 0. It is obvious that the ESMRL can improve the response and reduce the chattering phenomenon of the system.

Taking the first term of the ESMRL into consideration, we can obtain the simplified ESMRL as follows:

$$\dot{s} = -\frac{\varepsilon}{\delta + \left(1 + \frac{1}{|x|^n} - \delta\right) e^{-\alpha |s|}} \operatorname{sgn}(s) \tag{12}$$

Assumption 4: t_{rtn} is the required time for the error vector to reach the sliding-mode surface, and $s(t_{rte}) = 0$.

Thus equation (12) can be written as follows:

$$\dot{s}\left[\delta + \left(1 + \frac{1}{|x|^n} - \delta\right) e^{-\alpha |s|}\right] = -\varepsilon \operatorname{sgn}(s) \tag{13}$$

By integrating equation (13) from 0 to t_{rte}, the following can be obtained

$$\int_{s(0)}^{s(t_{rte})} \frac{1}{\operatorname{sgn}(s)} \left[\delta + \left(1 + \frac{1}{|x|^n} - \delta\right) e^{-\alpha |s|}\right] ds = \int_0^{t_{rte}} -\varepsilon dt \tag{14}$$

Then

$$t_{rte} = \frac{1}{\varepsilon} \left[\delta |s(0)| - \left(1 + \frac{1}{|x|^n} - \delta\right) \int_{s(0)}^{s(t_{rte})} \operatorname{sgn}(s) e^{-\alpha |s|} ds\right] \tag{15}$$

If $s \geq 0$, then

$$t_{rte} = \frac{1}{\varepsilon} \left[\delta s(0) + \frac{1}{\alpha} \left(1 + \frac{1}{|x|^n} - \delta\right) \left(1 - e^{-\alpha s(0)}\right)\right] \tag{16}$$

In contrast, if $s \leq 0$, then

$$t_{rte} = \frac{1}{\varepsilon} \left[-\delta s(0) + \frac{1}{\alpha} \left(1 + \frac{1}{|x|^n} - \delta\right) \left(1 - e^{\alpha s(0)}\right)\right] \tag{17}$$

Combining equations (16) and (17), the expression can be rewritten as

$$t_{rte} = \frac{1}{\varepsilon} \left[\delta |s(0)| + \frac{1}{\alpha} \left(1 + \frac{1}{|x|^n} - \delta\right) \left(1 - e^{-\alpha |s(0)|}\right)\right] \tag{18}$$

Since $1 - e^{-\alpha |s(0)|} < 1$, it can be known that

$$t_{rte} < \frac{1}{\varepsilon} \left[\delta |s(0)| + \frac{1}{\alpha} \left(1 + \frac{1}{|x|^n} - \delta\right)\right] \tag{19}$$

Thus, if parameter α is chosen appropriately, equation (19) can be derived as

$$t_{rte} < \frac{\delta |s(0)|}{\varepsilon} \tag{20}$$

Since δ is a strictly positive offset that is less than one, and $\varepsilon_0 = \varepsilon$, this means that

$$t_{rte} < t_{rtc} \tag{21}$$

In summation, the reaching time of the first term is less than the CSMRL. In addition, the second term of the ESMRL can also accelerate the reaching speed of the ESMRL. Thus the ESMRL has a faster dynamic response than that of the CSMRL.

The discrete form of ESMRL can be written as

$$\begin{aligned} s(n+1) - s(n) = &-\frac{\varepsilon T}{\delta + \left(1 + \frac{1}{|x|^n} - \delta\right) e^{-\alpha |s(n)|}} \\ &\times \operatorname{sgn}(s(n)) - \eta |x|^m T s(n) \end{aligned} \tag{22}$$

where T is the sampling period.

$$\begin{cases} s(n+1) = -\dfrac{\varepsilon |x|^n T}{1 + |x|^n}, & s(n) = 0^+ \\ s(n+1) = \dfrac{\varepsilon |x|^n T}{1 + |x|^n}, & s(n) = 0^- \end{cases} \tag{23}$$

Thus, the discrete sliding-mode boundary width of the ESMRL is as follows:

$$\Delta_{ESMRL} = \frac{2\varepsilon T\,|x|^n}{1+|x|^n} \tag{24}$$

The selection of parameters satisfies the following rules:

$$\varepsilon_0 = \varepsilon \tag{25}$$

$$T_0 = T \tag{26}$$

Obviously, the following equation can be obtained:

$$\Delta_{ESMRL} < \Delta_{CSMRL} \tag{27}$$

Compared with the CSMRL, where the bandwidth is constant, the bandwidth of the ESMRL can decrease as the value of $|x|$ decreases. Consequently, the chattering phenomena can be effectively mitigated by the enhanced sliding-mode reaching law.

IV. DESIGN OF CLAMPING FORCE CONTROLLER BASED ON ESMRL

A. CONTROL STRATEGIES FOR THE GAP DISTANCE

1) ELIMINATION STRATEGY FOR THE GAP DISTANCE

The block diagram for the EMB control strategy is shown in Fig. 4.

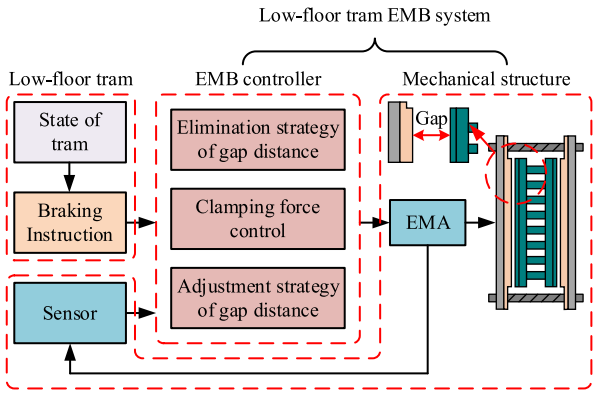

FIGURE 4. Block diagram of the EMB control strategy.

When the EMB controller receives the braking instruction, the EMB system eliminates the gap distance rapidly. Then, the EMB controller switches to the clamping force control, and the control algorithm switching point is detected by the position sensor.

During the period of eliminating the gap distance, the load of the drive motor is approximately nil. Therefore, the gap distance elimination strategy adopts constant torque control, which is based on a conventional PI control algorithm. This can be realized through a strategy where the drive motor can reach the maximum no-load speed quickly, and the gap distance can be eliminated in the possible time. Meanwhile, because the drive motor is characterized by low voltage and high current, it has a large starting current when the EMB system engages. This strategy can prevent the impact of an excessive starting current on the power grid of the low-floor tram.

2) ADJUSTMENT STRATEGY FOR THE GAP DISTANCE

The gap distance will increase as the brake pad and disc degrade with use. This phenomenon will increase the time required to eliminate the gap distance. The difference can lead to the response time of the EMB system becoming inconsistent in the same low-floor tram, which could lead to low-floor tram derailments. The adjustment strategy of gap distance is proposed and shown in Fig. 5.

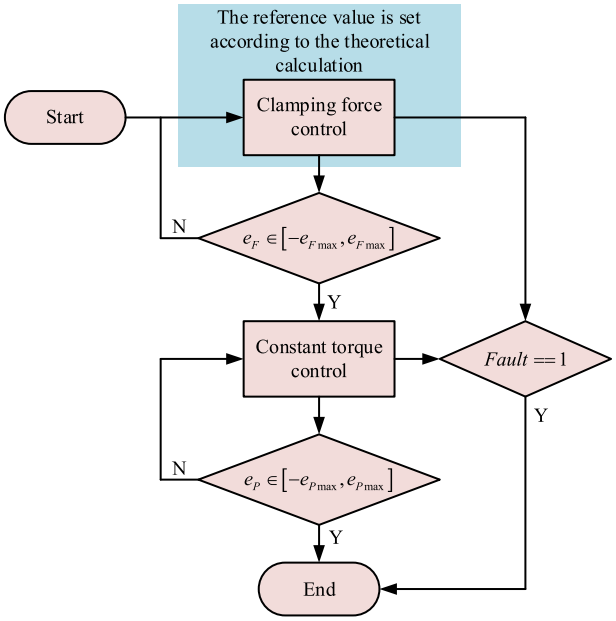

FIGURE 5. The adjustment strategy of gap distance.

When the adjustment instruction of the gap distance is received by the EMB controller, the system will track the target value, which is set according to theoretical calculations. Then, if the error of the system satisfies the desired error band, the system will use constant torque to control the drive motor reverse at a certain angle and adjust the gap distance to the expected value.

The measured value of the external laser range finder is taken as a reference, and the system can maintain the gap distance at 2 mm. The relevant parameters in the test are shown in Table 1, and the error curve is shown in Fig. 6.

TABLE 1. Parameters of the adjustment strategy.

Parameters	Value
Target clamping force	5 kN
Error band	[-200 N,200 N]
Fallback Hall count	200

In Fig. 6, we can see that the gap distance can be maintained at 2 mm for the drive motor at the backward 200 Hall number, when the measured clamping force is in the error band set for the adjustment of gap distance. This control strategy does not depend on an external mechanical structure,

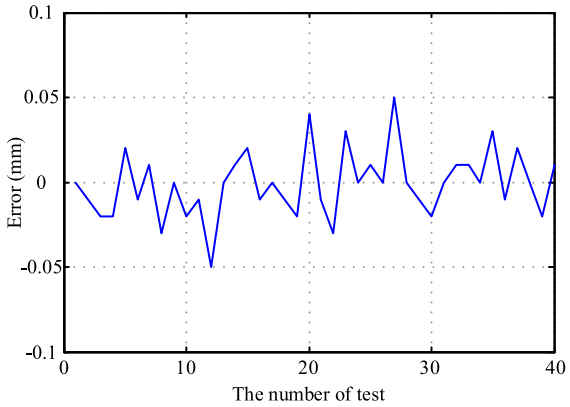

FIGURE 6. The error curve of the adjustment strategy.

and it can make the EMB system compensate for the abrasion of the brake disc and pad automatically. The approach is simple and practical.

B. CLAMPING FORCE CONTROLLER BASED ON ESMRL

The clamping force controller of the EMB is used to track the reference clamping force accurately and is robust to parameters such as external load disturbance.

The status variables of the EMB system are expressed as:

$$\begin{cases} x_1 = F_{ref} - F \\ x_2 = \dot{x}_1 = \dot{F}_{ref} - \dot{F} \end{cases} \tag{28}$$

where, F_{ref} represents the reference clamping force and F represents the actual clamping force.

When considering the contact state between the brake pad and disc, the clamping force error equation is described as:

$$\begin{cases} \dot{x}_1 = \dot{F}_{ref} - a\omega_m \\ \dot{x}_2 = \ddot{F}_{ref} - \dfrac{a}{J}\left(K_T i - T_L - B_v\omega_m\right) \end{cases} \tag{29}$$

where, $a = k_s L_0/2\pi GR$ and T_L represents the load torque.

To reduce the steady-state error and improve the robustness of the system, the integral sliding-mode surface is designated as

$$s = cx_1 + x_2 + \zeta \int_0^t x_1 dt \tag{30}$$

where, c and ζ are positive constant.

Based on the ESMRL, the virtual control quantity i^* can be designed as:

$$i^* = \frac{J}{aK_T}\begin{bmatrix} cx_2 + \ddot{F}_{ref} + \dfrac{a}{J}T_L + \dfrac{a}{J}B_v\omega_m + \zeta x_1 \\ +\Psi\left(x, s\right)\operatorname{sgn}\left(s\right) + \eta\left|x\right|^m s \end{bmatrix} \tag{31}$$

To verify the stability of the designed clamping force controller based on the ESMRL, the *Lyapunov* function is defined as:

$$V = \frac{1}{2}s^2 \tag{32}$$

TABLE 2. Parameters of the EMB system.

Parameters	Unit	Value
Rated Voltage V_{DC}	V	24
Rated Current I	A	45
Rated Torque T_e	N·m	2.96
Rated Speed	rpm	3028
Stator Resistance R_m	Ω	0.01
Stator Inductance L	H	3.3648×10^{-7}
Pole Pairs P		4
Gear Ratio		40:1
Ball Screw Ball L_0	mm	10
Stiffness Coefficient k_{sc}	kN/mm	47

Combined with equations (11) and (31), the derivative of the *Lyapunov* function (32) can be expressed as

$$\begin{aligned} \dot{V} &= s\dot{s} \\ &= s\left(\zeta x_1 + cx_2 + \dot{x}_2\right) \\ &= s\left[\zeta x_1 + cx_2 + \ddot{F}_{ref} - \frac{a}{J}\left(K_T i^* - T_L - B_v\omega_m\right)\right] \\ &= s\left[-\Psi\left(x, s\right)\operatorname{sgn}\left(s\right) - \eta\left|x\right|^m s\right] \\ &= -\Psi\left(x, s\right)\left|s\right| - \eta\left|x\right|^m s^2 \end{aligned} \tag{33}$$

In equation (33), due to $\varepsilon > 0$, $\eta > 0$, and $0 < \delta < 1$, $\dot{V} \leq 0$ can be established.

When there is an error in the system, we can do the following analysis:

(1) If $s = 0$, the system error will converge to zero along with the sliding-mode surface.

(2) If $s \neq 0$, $\dot{V} < 0$ can be established. The system will reach the sliding-mode surface in finite time.

Therefore, according to the *Lyapunov* stability theorem, the optimization controller is global asymptotically stable, and it can guarantee the system reaching the sliding-mode face.

V. SIMULATION AND EXPERIMENT RESULTS

A. SIMULATION RESULTS AND ANALYSIS

The MATLAB(2019a)/Simulink platform is utilized to illustrate the superiority and feasibility of the proposed control strategy in the EMB system. Meanwhile, the parameters of the EMB system are shown in Table 2, which are used in the simulation.

The parameters of the proposed control strategy are $\varepsilon = 1200$, $\delta = 0.6$, $n = 1$, $\alpha = 60$, $\eta = 100$ and $m = 1.5$. The parameters of the CSMRL controller are $\varepsilon_0 = 2000$. The parameters of the NSMRL controller are $\varepsilon_N = 1500$, $\delta_N = 0.6$, $\gamma_N = 5$ and $\alpha_N = 40$. The parameters of sliding-mode surface is set as $c = 100$, $\zeta = 45$. The parameters of the clamp force PI controller are $k_{Pf} = 4$, $k_{Pf} = 0.2$. The parameter of the current PI controller are the same as $k_{Pc} = 1.25$, $k_{Ic} = 0.1$.

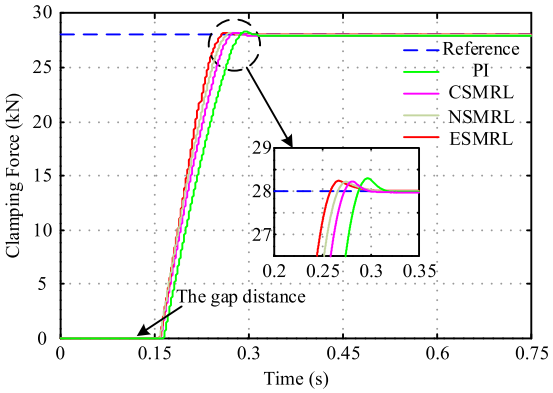

FIGURE 7. Simulation results of the step clamping force signal tracking with different control strategies.

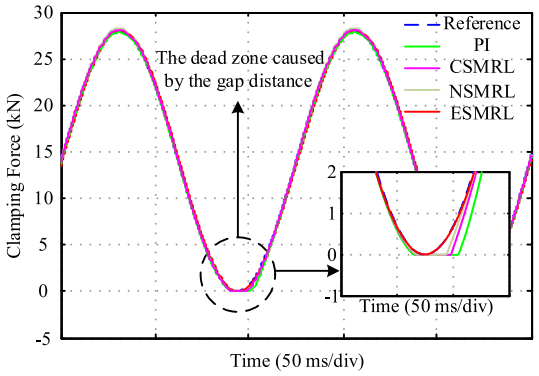

FIGURE 8. Simulation results of sinusoidal clamping force signal tracking with different control strategies.

***Case 1*:** To verify the dynamic response of the ESMRL, simulations of the clamping force step response are performed. The gap distance of the EMB system is set as 2 mm, and the reference clamping force signal is 28 kN.

In Fig. 7, it can be seen that the clamping force of the three control strategies are finally stable. The clamping force response time of the ESMRL is 235 ms, which is faster than the other control strategies. Therefore, compared with other control strategies, the proposed control strategy can achieve a stable state quickly and possesses excellent dynamic response performance. Table 3 shows the simulation results of the step response.

TABLE 3. Simulation results of the step response.

Control Strategy	Response Time
PI	264 ms
CSMRL	249 ms
NSMRL	241 ms
ESMRL	235 ms

***Case 2*:** In this case, a comparison of the dynamic tracking performance is performed. Fig. 8 shows the simulation results for tracking of the sinusoidal clamping force signal tracking and simulation results with different strategies. The reference clamping force signal is set as $F^* = 28\sin(4\pi t)$kN.

Due to the existence of a gap distance and the different dynamic tracking performances, the brake pad will leave the brake disc at different degrees. This is the reason why there is a dead zone at 0 in the sinusoidal reference clamping force signal. As seen in Fig. 8, the proposed control strategy achieves a superior tracking performance of sinusoidal clamping force signal than the other control strategies. Comparing the simulation results with different control strategies, the proposed control strategy provides better tracking of the reference signal and ensures the disappearance of the dead zone at the critical point. Therefore, the ESMRL has fewer clamping force dynamic tracking errors than the other two control strategies under the same conditions.

B. EXPERIMENTAL RESULTS AND ANALYSIS

To further illustrate the effectiveness of the proposed control strategy, experimental tests based on the EMB system of the tram are performed.

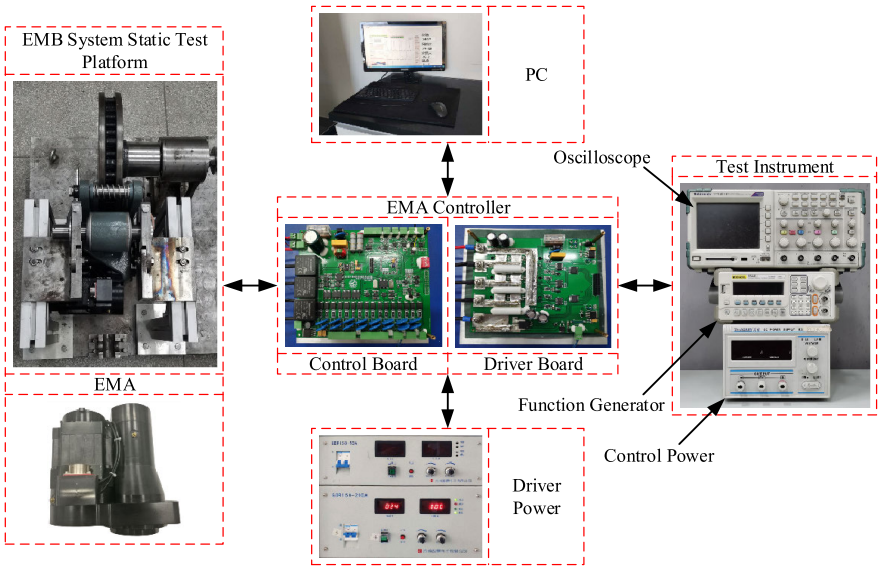

FIGURE 9. Structure of the EMA.

TABLE 4. Experimental results of the step response.

Control Strategy	Response Time
PI	427 ms
CSMRL	342 ms
NSMRL	327 ms
ESMRL	303 ms

Experiments are conducted on an EMB system static test platform whose parameters are consistent with Table 2. The experimental platform of the EMB system is shown in Fig. 9, which consists of an EMB bench, EMA controller, EMB control platform, data storage oscilloscope and DC power supply. The DC power supply is available at 24 V. The detailed information of the EMA controller is as follows: the main control chip is a TMS320F2812 digital signal processor (DSP); a UCC27211 half-bridge driver is selected as the gate driver; the three-phase inverter bridge circuit consists of the N-channel MOSFET transistor CSD19506KCS with a frequency of 10 kHz. In the experiments, the reference signal is generated by a RIGOL DG1022U function generator, and the actual clamping force signal is converted into a voltage signal by the EMA controller, which is measured by a Tektronix TPS2014B oscilloscope. A Tektronix A622 current probe is used to measure the busbar current. The gap distance of the static test is set as 2 mm.

The parameters of the proposed control strategy are $\varepsilon = 765$, $\delta = 0.6$, $n = 1$, $\alpha = 13$, $\eta = 137$ and $m = 1.5$. The parameters of the CSMRL controller are $\varepsilon_0 = 1175$. The parameters of the NSMRL controller are $\varepsilon_N = 943$, $\delta_N = 0.6$, $\gamma_N = 3$ and $\alpha_N = 37$. The parameters of sliding-mode surface are set as $c = 67$, $\zeta = 29$. The parameters of the clamp force PI controller are $k_{Pf} = 25$, $k_{If} = 0.0025$. The parameters of the current PI controller are the same as $k_{Pc} = 3$, $k_{Ic} = 0.01$.

***Case 1*:** In this case, the response rate and steady-state error of the EMB system are compared based on PI control, CSMRL control, NSMRL control and ESMRL control, which is achieved through the step response experiment.

***Experimental conditions*:** (1) The gap distance between the brake pad and disc is adjusted to 2 mm. (2) The reference signal of the step response is set as 28 kN.

The experiment results with different control strategies are shown in Fig. 10 (a)-(d).

As shown in Fig. 10, the maximum overshoot of the ESMRL control is less than other control strategies. It can also be seen from the busbar current that the current fluctuation is minimal when the ESMRL control is adopted in a steady state. It is obvious that the ESMRL control improves the control precision of the EMB system, and the energy utilization efficiency of the low-floor tram, which reduce the frequency of adjustment. A comparison of the response rates are shown in Table 4.

The results in Table 4 show that the ESMRL control achieves the fastest response rate under the minimum overshoot. This shows that the proposed control strategy has good response performance.

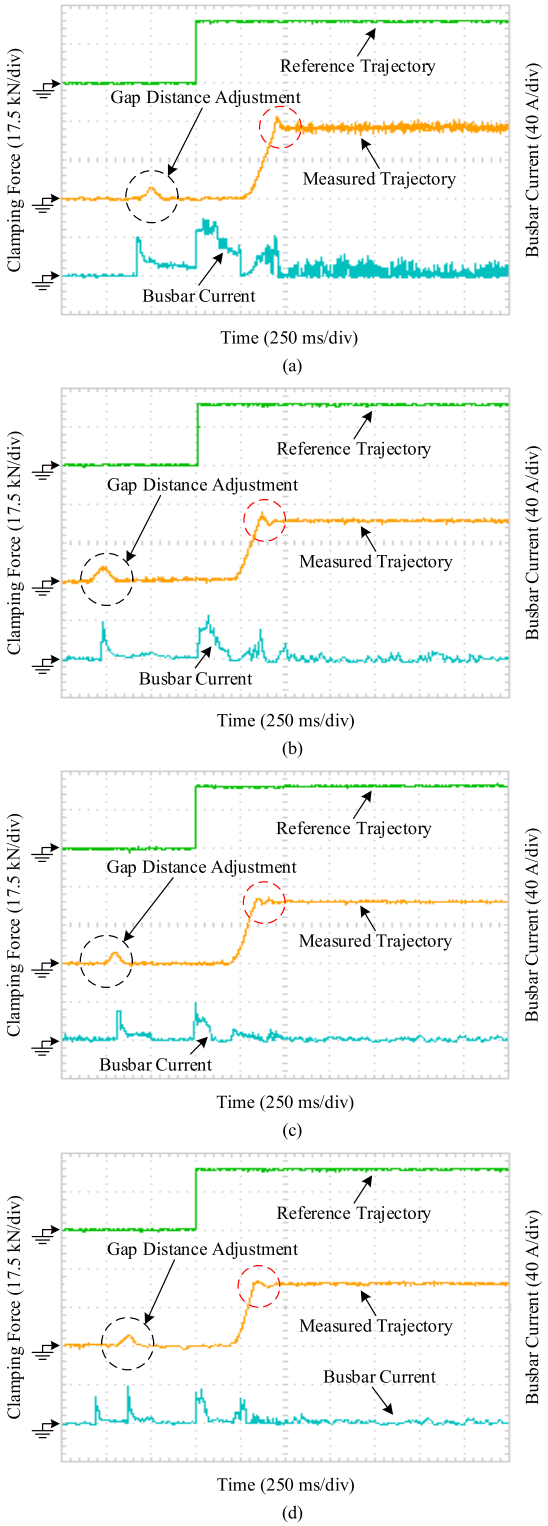

FIGURE 10. Experimental results of the step clamping force signal tracking with different control strategies. (a) Experimental results under PI controller. (b) Experimental results under CSMRL controller. (c) Experimental results under NSMRL controller. (d) Experimental results under ESMRL controller.

***Case 2*:** To verify the dynamic performance of the ESMRL, the reference signal is set as $F^* = 28 \sin(4\pi t)$kN. The tracking trajectories of the four methods—PI, CSMRL, NSMRL and ESMRL—are shown in Fig. 11.

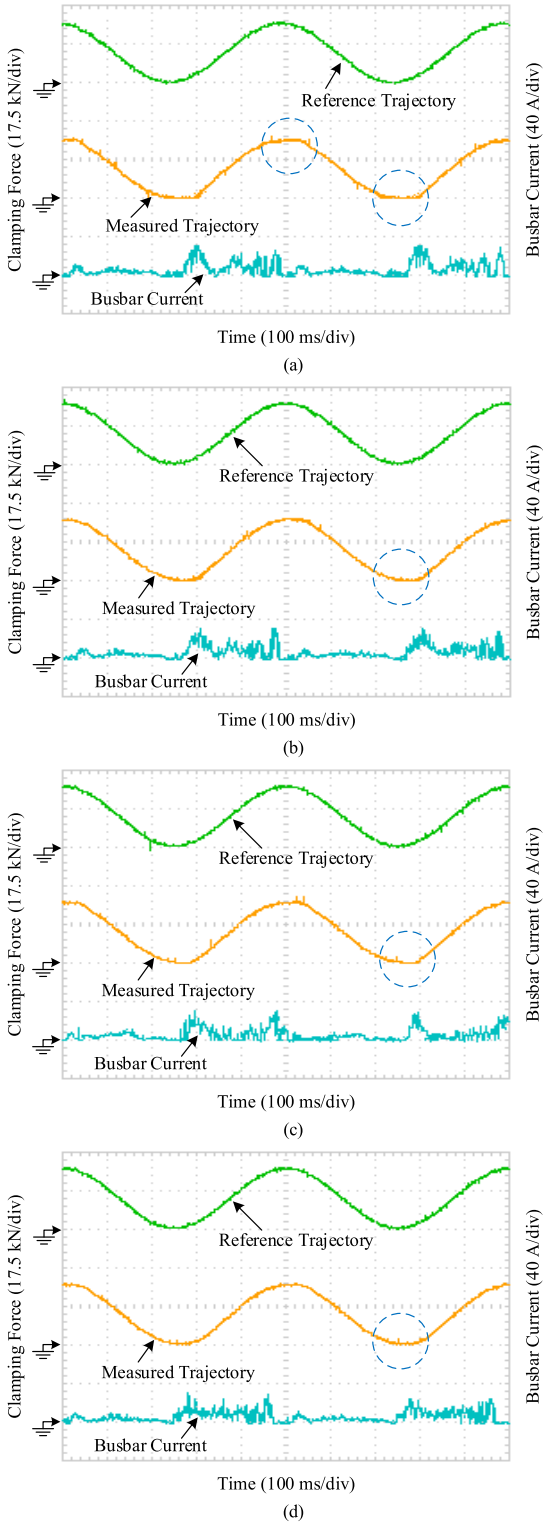

FIGURE 11. Experimental results of the sinusoidal clamping force signal tracking with different control strategies. (a) Experimental results under PI controller. (b) Experimental results under CSMRL controller. (c) Experimental results under NSMRL controller. (d) Experimental results under ESMRL controller.

As shown in Fig. 11 (a)-(d), it can be seen that the proposed method has a smoother clamping force and bus bar current trajectory compared to the other control strategies. At the critical point of contact between the brake pad and disc, the hysteresis is notably improved, when the ESMRL control is adopted. It obvious that the proposed control strategy can perfect the dynamic performance of the EMB system. The release of the brake pad from the brake disc is avoided when tracking the sinusoidal reference signal.

According to above experiments, it is verified that the proposed method achieves a high position tracking accuracy and good anti-interference performance.

VI. CONCLUSION

In this paper, a novel clamping force sliding-mode control strategy and gap distance control strategies are proposed for an EMB system with the characteristics of load torque variations, strong nonlinearity and complex structure. The main contributions of this paper are as follows:

(1) A mathematical model is established that focuses on the EMB system of a low-floor tram.

(2) An ESMRL is proposed to improve the clamping force control performance of an EMB system. Compared with the CSMRL, the ESMRL can decrease the convergence of reaching time to the sliding-mode surface and mitigate the chattering phenomena.

(3) A novel gap distance elimination strategy is proposed to shorten the response time of the EMB system.

(4) The proposed adjustment strategy accurately controls the gap distance and ensures the response time after the degradation the brake pad and disc.

Furthermore, the effectiveness and superiority of the proposed approach are validated by both simulations and experiments; the results show that the control strategy proposed in this paper can improve the dynamic performance and tracking accuracy of the clamping force control.

In future work, we will design different EMB systems for different railway vehicles. With a focus on the differences among different systems, we will summarize the tuning rules of ESMRL parameters for different nonlinear systems and improve the efficiency of parameter modulation.

REFERENCES

[1] W. Ding and X. Song, "Analysis of the anti-kink hydraulic system and running mode of low-floor trams," *J. Eng.*, vol. 2020, no. 14, pp. 966–969, 2020.

[2] X. Wang, Q. Wang, and S. Liang, "Predictive control algorithm for urban rail train brake control system based on T-S fuzzy model," *Comput., Mater. Continua*, vol. 64, no. 3, pp. 1859–1867, 2020.

[3] M. Khodaparastan, A. A. Mohamed, and W. Brandauer, "Recuperation of regenerative braking energy in electric rail transit systems," *IEEE Trans. Intell. Transp. Syst.*, vol. 20, no. 8, pp. 2831–2847, Aug. 2019.

[4] M. L. Wu, T. H. Ma, J. Yang, and M. L. Chen, "Discussion on development trend of train braking technology," *China Railway Sci.*, vol. 40, no. 1, pp. 134–144, Jan. 2019.

[5] S. E. Lyshevski, V. A. Skormin, and R. D. Colgren, "High-torque density integrated electro-mechanical flight actuators," *IEEE Trans. Aerosp. Electron. Syst.*, vol. 38, no. 1, pp. 174–182, Jan. 2002.

[6] P. Krishnamurthy, W. Lu, F. Khorrami, and A. Keyhani, "Robust force control of an SRM-based electromechanical brake and experimental results," *IEEE Trans. Control Syst. Technol.*, vol. 17, no. 6, pp. 1306–1317, Nov. 2009.

[7] Y. O. Lee, Y. S. Son, and C. C. Chung, "Clamping force control for an electric parking brake system: Switched system approach," *IEEE Trans. Veh. Technol.*, vol. 62, no. 7, pp. 2937–2948, Sep. 2013.

[8] C. Jo, S. Hwang, and H. Kim, "Clamping-force control for electromechanical brake," *IEEE Trans. Veh. Technol.*, vol. 59, no. 7, pp. 3205–3212, Sep. 2010.

[9] C. F. Lee and C. Manzie, "Active brake judder attenuation using an electromechanical brake-by-wire system," *IEEE/ASME Trans. Mechatronics*, vol. 21, no. 6, pp. 2964–2976, Dec. 2016.

[10] C. Line, C. Manzie, and M. C. Good, "Electromechanical brake modeling and control: From PI to MPC," *IEEE Trans. Control Syst. Technol.*, vol. 16, no. 3, pp. 446–457, May 2008.

[11] Y. Sun, J. Xu, H. Qiang, and G. Lin, "Adaptive neural-fuzzy robust position control scheme for maglev train systems with experimental verification," *IEEE Trans. Ind. Electron.*, vol. 66, no. 11, pp. 8589–8599, Nov. 2019.

[12] Y. Sun, J. Xu, G. Lin, W. Ji, and L. Wang, "RBF neural network-based supervisor control for maglev vehicles on an elastic track with network time-delay," *IEEE Trans. Ind. Informat.*, early access, Oct. 19, 2020, doi: 10.1109/TII.2020.3032235.

[13] S. Mobayen and J. Ma, "Robust finite-time composite nonlinear feedback control for synchronization of uncertain chaotic systems with nonlinearity and time-delay," *Chaos, Solitons Fractals*, vol. 114, pp. 46–54, Sep. 2018.

[14] X. Wang, W. Wang, L. Li, J. Shi, and B. Xie, "Adaptive control of DC motor servo system with application to vehicle active steering," *IEEE/ASME Trans. Mechatronics*, vol. 24, no. 3, pp. 1054–1063, Jun. 2019.

[15] C. Liu, G. Luo, X. Duan, Z. Chen, Z. Zhang, and C. Qiu, "Adaptive LADRC-based disturbance rejection method for electromechanical servo system," *IEEE Trans. Ind. Appl.*, vol. 56, no. 1, pp. 876–889, Jan. 2020.

[16] W.-L. Zhu, X. Yang, F. Duan, Z. Zhu, and B.-F. Ju, "Design and adaptive terminal sliding mode control of a fast tool servo system for diamond machining of freeform surfaces," *IEEE Trans. Ind. Electron.*, vol. 66, no. 6, pp. 4912–4922, Jun. 2019.

[17] C.-Y. Lin and Y.-C. Liu, "Precision tracking control and constraint handling of mechatronic servo systems using model predictive control," *IEEE/ASME Trans. Mechatronics*, vol. 17, no. 4, pp. 593–605, Aug. 2012.

[18] Y. B. Shtessel, J. A. Moreno, and L. M. Fridman, "Twisting sliding mode control with adaptation: Lyapunov design, methodology and application," *Automatica*, vol. 75, pp. 229–235, Jan. 2017.

[19] A. Al-Durra, "Adaptive sliding mode observer for engine cylinder pressure imbalance under different parameter uncertainties," *IEEE Access*, vol. 2, pp. 1085–1091, Sep. 2014.

[20] A. Bartoszewicz and P. Latosinski, "Reaching law based discrete time sliding mode inventory management strategy," *IEEE Access*, vol. 4, pp. 10051–10058, Jan. 2016.

[21] S. Mobayen, "Design of LMI-based sliding mode controller with an exponential policy for a class of underactuated systems," *Complexity*, vol. 21, no. 5, pp. 117–124, May/Jun. 2016.

[22] C. Gong, Y. Hu, J. Gao, Y. Wang, and L. Yan, "An improved delay-suppressed sliding-mode observer for sensorless vector-controlled PMSM," *IEEE Trans. Ind. Electron.*, vol. 67, no. 7, pp. 5913–5923, Jul. 2020.

[23] M. Jin, J. Lee, P. Hun Chang, and C. Choi, "Practical nonsingular terminal sliding-mode control of robot manipulators for high-accuracy tracking control," *IEEE Trans. Ind. Electron.*, vol. 56, no. 9, pp. 3593–3601, Sep. 2009.

[24] S. Mobayen, S. Mostafavi, and A. Fekih, "Non-singular fast terminal sliding mode control with disturbance observer for underactuated robotic manipulators," *IEEE Access*, vol. 8, pp. 198067–198077, Nov. 2020.

[25] D. K. Giri and M. Sinha, "Finite-time continuous sliding mode magneto-Coulombic satellite attitude control," *IEEE Trans. Aerosp. Electron. Syst.*, vol. 52, no. 5, pp. 2397–2412, Oct. 2016.

[26] Y. Sun, J. Xu, H. Qiang, C. Chen, and G. Lin, "Adaptive sliding mode control of maglev system based on RBF neural network minimum parameter learning method," *Measurement*, vol. 141, pp. 217–226, Jul. 2019.

[27] V. Acary, B. Brogliato, and Y. V. Orlov, "Chattering-free digital sliding-mode control with state observer and disturbance rejection," *IEEE Trans. Autom. Control*, vol. 57, no. 5, pp. 1087–1101, May 2012.

[28] A. Saghafinia, H. W. Ping, M. N. Uddin, and K. S. Gaeid, "Adaptive fuzzy sliding-mode control into chattering-free IM drive," *IEEE Trans. Ind. Appl.*, vol. 51, no. 1, pp. 692–701, Jan. 2015.

[29] S. Mobayen and F. Tchier, "Nonsingular fast terminal sliding-mode stabilizer for a class of uncertain nonlinear systems based on disturbance observer," *Scientia Iranica*, vol. 24, no. 3, pp. 1410–1418, Jun. 2017.

[30] Y. Feng, F. Han, and X. Yu, "Chattering free full-order sliding-mode control," *Automatica*, vol. 50, no. 4, pp. 1310–1314, Apr. 2014.

[31] A. K. Junejo, W. Xu, C. Mu, M. M. Ismail, and Y. Liu, "Adaptive speed control of PMSM drive system based a new sliding-mode reaching law," *IEEE Trans. Power Electron.*, vol. 35, no. 11, pp. 12110–12121, Nov. 2020.

[32] S. Yi and J. Zhai, "Adaptive second-order fast nonsingular terminal sliding mode control for robotic manipulators," *ISA Trans.*, vol. 90, pp. 41–51, Jul. 2019.

[33] M. Ye and H. Wang, "A robust adaptive chattering-free sliding mode control strategy for automotive electronic throttle system via genetic algorithm," *IEEE Access*, vol. 8, pp. 68–80, Jan. 2020.

[34] W. Gao and J. C. Hung, "Variable structure control of nonlinear systems: A new approach," *IEEE Trans. Ind. Electron.*, vol. 40, no. 1, pp. 45–55, Feb. 1993.

[35] Y. Wang, Y. Feng, X. Zhang, and J. Liang, "A new reaching law for antidisturbance sliding-mode control of PMSM speed regulation system," *IEEE Trans. Power Electron.*, vol. 35, no. 4, pp. 4117–4126, Apr. 2020.

[36] B. Brahmi, M. H. Laraki, A. Brahmi, M. Saad, and M. H. Rahman, "Improvement of sliding mode controller by using a new adaptive reaching law: Theory and experiment," *ISA Trans.*, vol. 97, pp. 261–268, Feb. 2020.

[37] L. Tao, Q. Chen, Y. Nan, and C. Wu, "Double hyperbolic reaching law with chattering-free and fast convergence," *IEEE Access*, vol. 6, pp. 27717–27725, Jun. 2018.

[38] D. H. Shin, T. S. Park, S. H. Jin, J. I. Moon, and S. H. Yang, "Study of mechanism for wear adjustment with electro wedge brake," *Key Eng. Mater.*, vol. 625, pp. 712–716, Aug. 2014.

[39] S. Lin, Y. Cai, B. Yang, and W. Zhang, "Electrical line-shafting control for motor speed synchronisation using sliding mode controller and disturbance observer," *IET Control Theory Appl.*, vol. 11, no. 2, pp. 205–212, Jan. 2017.

YIYUN ZHAO received the B.E. degree in electrical engineering from Northwestern Polytechnical University, Xi'an, China, in 2017, where he is currently pursuing the Ph.D. degree with the School of Automation. His research interests include nonlinear control and mechatronic servo control.

HUI LIN was born in 1957. He received the B.S. and M.S. degrees in electrical engineering and the Ph.D. degree in control science engineering from Northwestern Polytechnical University, in 1982, 1985, and 1993, respectively. He is a currently a Professor with the Department of Electrical Engineering, Northwestern Polytechnical University. His research interests include power electronics, electric vehicles, motion control, and control theory.

BINGQIANG LI received the B.E. and M.E. degrees in electrical engineering and the Ph.D. degree in control science and engineering from Northwestern Polytechnical University, Xi'an, China, in 2004, 2007, and 2010, respectively. He is currently an Associate Professor and the Dean of the Department of Electrical Engineering, Northwestern Polytechnical University, and a Postdoctoral Fellow with the Xi'an Aviation Brake Technology Company Ltd. His research interests include iterative learning control, fractional order control, servo control, multi-agent systems and their applications.